Ultrafast $Z \rightarrow E$ Photoisomerisation of Structurally Modified Furylfulgides

Falk Renth,[1,*] Ron Siewertsen,[1] Frank Strübe,[2] Jochen Mattay,[2] and Friedrich Temps[1,*]

[1] *Institut für Physikalische Chemie, Christian-Albrechts-Universität zu Kiel, Olshausenstr. 40, D-24098 Kiel, Germany*
[2] *Organische Chemie I, Fakultät für Chemie, Universität Bielefeld, Postfach 100131, D-33501 Bielefeld, Germany*

Femtosecond broadband transient absorption spectroscopy has been used in a comparative study of the ultrafast photo-induced $Z \rightarrow E$ isomerisation reactions of four photochromic furylfulgides with selected structural motifs in n-hexane as solvent. The results show that all studied Z-fulgides exhibit fast and direct processes along barrierless excited-state pathways involving a conical intersection (CI) between the S_1 and S_0 electronic states. The excited-state lifetimes range from $\tau_1 = 0.18$ ps for the methyl derivative to $\tau_1 = 0.32$ ps for the benzofurylfulgide. The impulsive rise of the absorption by vibrationally hot Z- and E-isomers back in the electronic ground state following electronic deactivation and isomerisation indicates that the initially prepared wave packet persists even after passage of the CI. Furthermore, the results provide qualitative evidence for a quickly dephasing vibrational coherence in the electronic ground state. In contrast to the significant changes observed for the corresponding E- and C-isomers [Renth *et al.*, *Int. Rev. Phys. Chem.* 2013, **32**, 1–38], the excited-state dynamics of the Z-isomers is not affected by varied sterical hindrance from methyl and isopropyl substituents at the central hexatriene unit, or by intramolecular bridging, and remains unaltered upon extension of the π-electron system in a benzannulated furyl fulgide.

Keywords: Molecular switches, fulgides, photochromism, isomerisation, femtosecond spectroscopy, ultrafast dynamics.

1. Introduction

Photochromic molecular switches are of considerable interest because of their enormous application potential, *e.g.* as functional building blocks in molecular devices and in information technology. In particular, fulgides are attractive because of fully reversible photoisomerisation reactions with high interconversion yields in combination with thermal irreversibility and high photostability.[1–10]

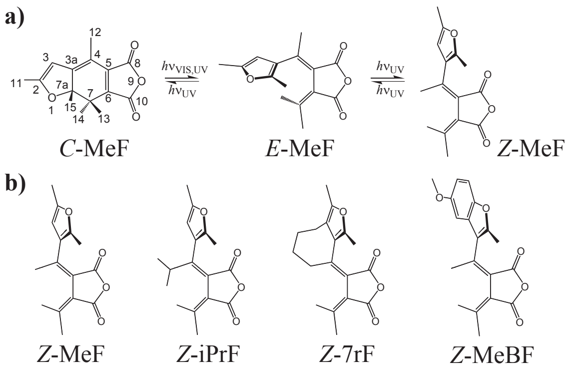

Fig. 1: a) Photoisomerisation reactions for the furylfulgide MeF. Atom numbering is indicated for C-MeF. b) Structures of the studied Z-isomers of fulgide derivatives MeF, iPrF, 7rF, and MeBF.

Figure 1a shows the photochemical reactions between the three isomers of compound MeF that has served as starting point for the striking structural evolution leading to the favourable photoswitching properties of modern fulgides.[8,10–14] The desired photochromic behaviour is based on the electrocyclic $E \rightarrow C$ ring closure of the colourless, open E-isomer and the reverse $C \rightarrow E$ ring opening of the coloured, closed C-isomer. The $E \rightarrow Z$ isomerisation is an unwanted side reaction that competes with the ring closure. Its potentially adverse effects on the performance of fulgide-based functional devices are, however, balanced by the reverse $Z \rightarrow E$ reaction, which effectively restores optical bistability by avoiding photochemical accumulation of the Z-isomer. This important feature allows for high $E \rightarrow C$ conversion yields, *e.g.* the photostationary state obtained by irradiation of E-MeF at 365 nm contains 95% C-MeF.[15]

While considerable synthetic efforts over several decades have demonstrated the potential of chemical structure to control the photoswitching in fulgides, recent comprehensive and systematic studies of the underlying photochromic reaction pathways have provided insight into the basis for the observed changes. Extensive work using ultrafast spectroscopy performed in our group for fulgides with selected structural motifs[10,16–20] (see Fig. 1b) and quantum chemical calculations[21–24] related the trends in photochemical behaviour upon structural variation to details of the underlying ultrafast photo-induced dynamics. Based on the experimental results, intramolecular bridging was introduced as a new structural motif to increase the quantum yields of the desired ring closure and block the $E \rightarrow Z$ isomerisation.[10,17–19] The improved properties of sterically constrained compounds such as iPrF or the bridged new derivative 7rF could be traced back to a favourable pre-orientation of the furyl unit for the conrotatory ring closure that accelerates the desired $E \rightarrow C$ reaction and enhances its efficiency. The $E \rightarrow Z$ photoisomerisation is effectively blocked by way of kinetic competition.

*Authors to whom correspondence should be addressed; renth@phc.uni-kiel.de, temps@phc.uni-kiel.de

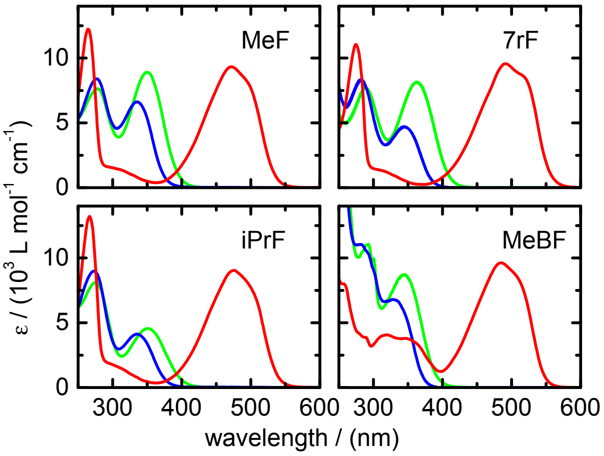

Fig. 2: UV/VIS absorption spectra of the *C*-, *E*-, and *Z*-isomers (red, blue and green lines) of MeF, iPr, 7rF, and MeBF in *n*-hexane.

In contrast, the excited-state dynamics of the photoexcited *C*-isomers is hardly affected by steric constraints, but slowed down up to ≈ 25 times upon extension of the π-electron system via benzannulation of the furyl moiety (compound MeBF).[20] Nevertheless, the ring opening quantum yield of *C*-MeBF turns out to be higher than for the other derivatives, suggesting distinctive reactive and unreactive pathways that are affected selectively by the electronic modification and involve excited-state energy barriers. Overall, the studies show that the ring closure and opening reactions of fulgide molecules can be tuned independently by intramolecular constraints and extension of the furyl π-electron system.[10]

Much less is known about the $Z \rightarrow E$ reaction. The only femtosecond time-resolved study so far showed an excited-state lifetime of 220 fs for *Z*-MeF excited at $\lambda_{\text{pump}} = 387$ nm. The results were interpreted in favour of a barrierless excited-state pathway leading to the electronic ground states of the *E*-isomer product and *Z*-isomer reactant molecules via a conical intersection (CI).[25] An apparent strongly damped oscillatory behaviour was tentatively interpreted as vibrational coherence. A comprehensive interpretation was prevented, however, by the limited spectral detection window and temporal resolution. This prompted us to extend our previous comparative studies of *E*- and *C*-fulgides with selected structural motifs to the corresponding *Z*-isomers (see Fig. 1b). As is evident from the UV/VIS absorption spectra in Fig. 2, photoexcitation into the first absorption bands should populate the same excited electronic states in all four derivatives, allowing for direct comparison of the resulting dynamics.

2. Experimental details

The syntheses of the four fulgides were published by Strübe *et al.*[17] The *Z*-isomers were isolated by column chromatography and recrystallisation in cyclohexane/ethyl acetate. Purities (> 98%) were checked by thin layer chromatography and by ^{1}H-NMR spectroscopy.

The femtosecond time-resolved broadband transient absorption measurements were done at room temperature using solutions of the *Z*-isomers in *n*-hexane (Uvasol, Merck) at an optical density of ≈ 0.3 in flow cells with optical path lengths of $d = 0.5$ mm for MeF, iPrF, and 7rF and $d = 1$ mm for MeBF. The experimental setup based on a regeneratively amplified Ti:Sa laser system (Clark CPA2001) has been described before.[16,25] The excitation pulses of 0.2 μJ at $\lambda_{\text{pump}} = 350$ nm came from a frequency-doubled home-built noncollinear optical parametric amplifier (NOPA). Broadband supercontinuum probe pulses between $\lambda_{\text{probe}} = 315$ and 655 nm were generated in CaF_2 and split into signal and reference beams. Their polarisation relative to the pump beam was set to the magic angle using a Berek variable wave plate. The pump-probe temporal delay was scanned with a computer-controlled linear translation stage in the probe path. The width of the instrument response function (IRF) determined from the cross-phase modulation (XPM) and stimulated Raman scattering (SRS) contributions was ≈ 40 fs (Gaussian standard deviation). XPM was also used to perform the time-zero correction, both XPM and SRS were subtracted from the data as described before.[16]

3. Results

3.1. Two-dimensional transient absorption maps

For a qualitative overview and comparison of the four fulgides, Fig. 3 shows the two-dimensional spectrotemporal transient absorption maps following excitation of the *Z*-fulgides at $\lambda_{\text{pump}} = 350$ nm for probe wavelengths between 315 nm $\leq \lambda_{\text{probe}} \leq$ 655 nm. All compounds display a very similar, complex behaviour comprising several distinctive components and dynamic spectral evolution. The strongly negative signals at probe wavelengths between 315 and 400 nm mirroring the respective absorption spectra (see Fig. 2 and top panels in Fig. 3) reflect the bleaching of the ground state absorption (GSB) by photoexcitation of the *Z*-isomers. The partial recovery of the ground state absorption (GSR) completes between 10 − 30 ps. GSB and possible negative contributions from stimulated emission (SE) are overlayed by a large-amplitude positive excited-state absorption (ESA) which extends over the entire spectral range and decays quickly within the first picosecond. In the wavelength range between $\lambda_{\text{probe}} = 380 - 475$ nm, an additional delayed rise appears to occur after ≈ 300 − 400 fs. This band narrows spectrally and shifts towards shorter wavelengths with increasing delay time. The behaviour and the position in the red wing of the longest-wavelength ground state absorption band suggests hot ground-state absorption (HGSA) from vibrationally excited *E*- and

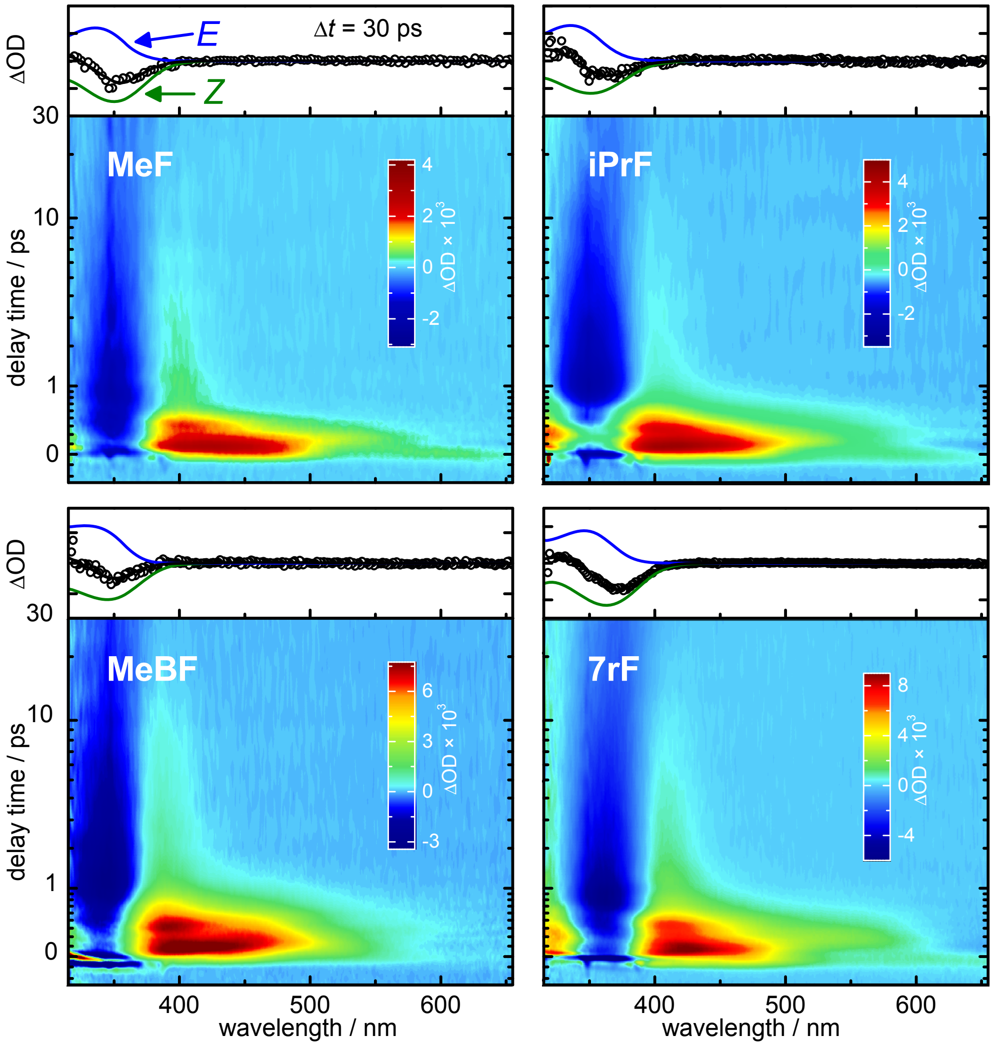

Fig. 3: Two-dimensional maps of the change in optical density ΔOD following excitation of the Z-fulgides at $\lambda_{\text{pump}} = 350$ nm for delay times (cf. Ref. 26) between -0.25 ps $\leq \Delta t \leq 30$ ps. Transient spectra at delay times $\Delta t = 30$ ps and their fits by a weighted sum of the static absorption spectra of the E- and Z-isomers are shown above the absorption maps.

Z-molecules returned to their electronic ground states as possible cause. The spectro-temporal changes reflect the vibrational cooling which is completed after $\Delta t \approx 20$ ps; no significant further evolution is seen beyond that delay time. The permanent absorption changes (PA) in the transient spectra at $\Delta t = 30$ ps depicted in the top panels of Fig. 3 can be described by the difference of the static E- and Z-isomer absorption spectra. No absorption related to formation of C-isomers could be detected.

3.2. Absorption-time profiles at fixed wavelengths

Further details of the photo-induced dynamics are revealed by the transient absorption time profiles at fixed probe wavelengths in Fig. 4 with photo-excited Z-MeF as representative example. For probe wavelengths from 575 to 400 nm, both the reactant Z-MeF and the product E-MeF do not show appreciable static UV/VIS absorption. Therefore GSB, its recovery (GSR), and permanent absorption changes (PA) play no role. The behaviour is dominated by the positive ESA that decays completely within ≈ 1 ps. At probe wavelengths $\lambda_{\text{probe}} \geq 475$ nm, the ESA does not rise in an IRF-limited fashion, but appears cropped close to its maximum, indicating a hidden negative component most likely due to SE (see also ESI). The profiles at $\lambda_{\text{probe}} < 475$ nm do not seem affected the same way, but display a shoulder in the decaying part of the ESA that grows in intensity with decreasing wavelength (*cf.* profile at $\lambda_{\text{probe}} = 420$ nm). Its slower decay within a few (up to ten) picoseconds and spectral signature suggest HGSA, *i.e.* strongly red-shifted ground state absorption of highly vibrationally excited E- and Z-molecules returned to the electronic ground state that undergo subsequent vibrational cooling as likely cause. To a lesser extent, the underlying spectro-temporal shifts

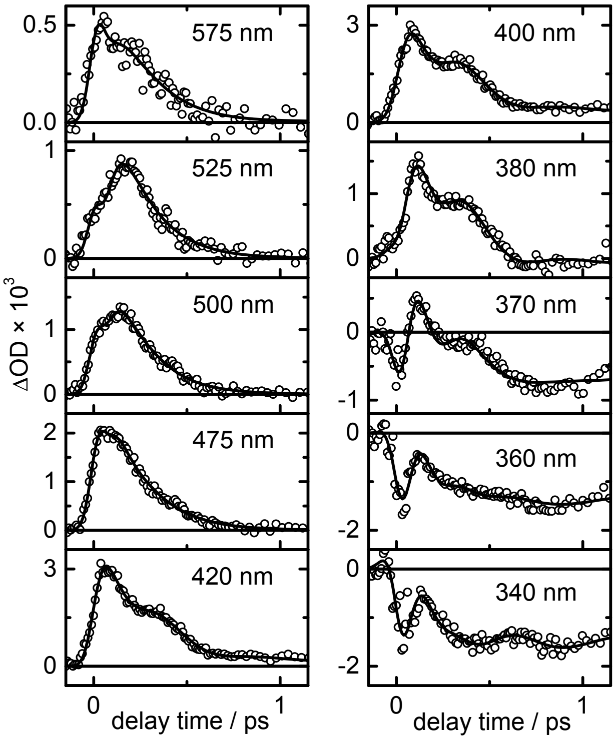

Fig. 4: Transient absorption time profiles following excitation of Z-MeF at $\lambda_{\mathrm{pump}} = 350$ nm. Open circles represent the data points, black lines the overall fits.

of the longest-wavelength UV/VIS absorption bands also show up in the time profiles from $\lambda_{\mathrm{probe}} = 380$ to 340 nm, which are increasingly affected by the strong initial GSB, GSR and the permanent absorption changes due to $Z \rightarrow E$ photoisomerisation. The profiles at the shortest probe wavelengths (370 to 340 nm) display a steep IRF-limited decay to negative transient absorption values followed by an intermediate maximum due to ESA located at $\Delta t \approx 0.2$ ps, *i.e.* slightly later than the corresponding maximum at longer probe wavelengths. This is evidence of a delayed rise of the positive ESA component in the UV probe range that could be caused, *e.g.* by a fast initial blue-shift of the underlying ESA band with maximum at visible wavelengths as result of the photo-induced wave-packet dynamics in the Franck-Condon region of the excited state. Finally, the slow rise of the absorption signals beyond $\Delta t \approx 0.75$ ps is related to HGSA and the partial recovery of the thermally equilibrated ground-state absorption by vibrational cooling.

3.3. Non-linear least-squares fit

For a reliable quantitative analysis of the data, simultaneous non-linear least-squares fitting of multiple time profiles at fixed probe wavelengths $\Delta OD_\lambda(t)$ was performed. A fit by weighted sums of exponential decays convolved with the instrument response function (IRF) gave no satisfactory results, in particular the fast rise of the delayed contributions was not captured well (see ESI). In addition, amplitude constraints or restriction of components to specific wavelength ranges could not be used to reduce the number of fit parameters and to break up their correlations, since the underlying decay associated difference spectra (DADS) are not related to individual components such as ESA or HGSA.

Target analysis[27] with species-associated components was thus mandatory. The previous qualitative analysis suggested a consecutive scheme,

$$Z \xrightarrow{h\nu} Z^* \longrightarrow \{E^\#, Z^\#\} \longrightarrow \{E, Z\}.$$

Starting with photo-excited Z^* molecules in the Franck-Condon (FC) region of the excited state, isomerisation and internal conversion to the electronic ground state yield vibrationally hot molecules in the electronic ground state $E^\#$ and $Z^\#$, which undergo vibrational cooling to the thermally equilibrated isomers E and Z. The target model based on this scheme includes ESA and SE as species-associated contributions by Z^* molecules in the excited state, HGSA by the vibrationally hot $\{E^\#, Z^\#\}$ ground state species, plus GSB, GSR and PA by thermally equilibrated Z- and E-molecules.

As has been discussed by Briand *et al.* for the $E \rightarrow Z$-isomerisation of a dipolar N-alkylated indanylidene-pyrroline (NAIP) photoswitch,[28–30] the fit model has to allow for the wave-packet nature of the molecules photo-excited by the ultrashort laser pulse. This results in an impulsive appearance of HGSA, GSR and the delayed ESA in the UV region that cannot be described by simple exponential kinetics derived from rate equations. In line with their approach,[28–30] the delayed onset of these components was described by time delays Δt, and the possibly slower rise was modelled by a Gaussian standard deviation σ slightly larger than the experimental time resolution of $\sigma_{\mathrm{IRF}} = 40$ fs. For GSB, SE, and ESA at visible probe wavelengths, σ_{IRF} was kept unchanged. The ESA decay and the HGSA time delay at different wavelengths were described by single global fit parameters τ_1 and Δt_{HGSA}. The HGSA decays were described by wavelength-dependent time constants τ_2 and τ_3 to take into account fast initial spectral evolution and slower vibrational cooling. GSR was modelled as delayed exponential rise with the same time constant τ_3. Finally, weak damped HGSA oscillations similar as observed in the NAIP case[28] were described by a global oscillation period T_{OSC} and a global damping time τ_{d}. The number of amplitude parameters was reduced by considering the following points (see ESI for further details):

(i) The GSB amplitudes at different wavelengths are related via the known static UV/VIS absorption spectrum of the Z-isomer and can be parametrized by the concentration of photo-excited Z-molecules c^*.

(ii) Fitting the PA at long delays by a weighted sum of the static E- and Z-isomer UV/VIS spectra (positive for the E product, negative for the Z reactant, see top panels of Fig. 3) yielded a weighting factor w_{ZE} that equals the product of the $Z \to E$ quantum yield ϕ_{ZE} and c^*. GSB can thus be expressed using ϕ_{ZE} (instead of c^*) as a single global parameter. For MeF and MeBF, the GSB amplitude is fixed, since $\phi_{ZE} = 0.11$ is known.[15,17]

(iii) Since GSR is the difference between GSB and PA, it is not an independent component. GSB, GSR and PA occur only at wavelengths with non-zero static UV/VIS absorption and are left out elsewhere. The amplitudes of ESA and HGSA are strictly positive, SE is negative.

The excellent description of the complex time evolutions for all four derivatives is seen in Fig. 5, where transient absorption time profiles representing the respective spectral regions are displayed along with their nonlinear least-squares fits and individual components. Table 1 collects the ESA decay times τ_1, HGSA delays Δt_{HGSA} and HGSA decay constants τ_2 and τ_3 (averaged for the indicated probe wavelength ranges) as most relevant fit parameters describing the temporal evolutions. The last column lists the fitted oscillation periods T_{OSC}.

Table 1: Fit results for the most important temporal parameters (2σ error limits in brackets unless otherwise indicated).

	τ_1/ps	Δt_{HGSA}/ps	τ_2/ps^{a,c}	τ_3/ps^{b,c}	T_{OSC}/ps	ϕ_{ZE}^{d}
MeF	0.18(1)	0.26(1)	0.18(3)	7.6(7)	0.54(2)	0.11
iPrF	0.26(1)	0.30(1)	0.21(5)	6.4(21)	0.45(2)	0.11(2)
7rF	0.26(1)	0.33(1)	0.29(3)	8.8(18)	0.52(2)	0.18(2)
MeBF	0.32(3)	0.33(1)	0.33(2)	6.4(12)	0.56(2)	0.11

^{a}Averaged from $\lambda_{\mathrm{probe}} = 420 - 475$ nm.
^{b}Averaged from $\lambda_{\mathrm{probe}} = 360 - 420$ nm.
^{c}Error limits by mean absolute deviation from average.
^{d}Set fixed to the static quantum yields for MeF and MeBF.[15,17]

Regarding the results, several remarks are in order:

(i) The steep initial IRF-limited decay and fast subsequent rise at UV probe wavelengths in the profiles at $\lambda_{\mathrm{probe}} = 360$ nm result from a slightly delayed and slower than IRF-limited rise of the ESA characterized by fit parameters $\Delta t_{\mathrm{ESA}} = 0.05 - 0.1$ ps and $\sigma_{\mathrm{ESA}} = 0.06 - 0.1$ ps. In line with a rapid blue-shift of the ESA, Δt_{ESA} and σ_{ESA} are largest at the shortest probe wavelengths.

(ii) The SE decay times increase to $\tau_{\mathrm{SE}} = 0.1 - 0.13$ ps at longer wavelengths. Fitting without SE deteriorates the data description and requires unphysical values of $\sigma_{\mathrm{IRF}} > 0.1$ ps (see ESI).

(iii) HGSA can be seen even at probe wavelengths up to $\lambda_{\mathrm{probe}} \approx 475$ nm, corresponding to red-shift of the ground state absorption by ≈ 70 nm. The related HGSA decay time τ_2 is of the same order as τ_1. The slower HGSA decay component τ_3 is present only at $\lambda_{\mathrm{probe}} \leq 420$ nm. HGSA at ≈ 360 nm contains contributions of E- and Z-isomers. Its behaviour reflects the differences in the position, intensity and spectral shifts of the respective ground-state absorption bands of the studied derivatives.

(iv) The PA, GSR and GSB amplitudes in the global fits depend on the isomerisation quantum yields ϕ_{ZE} as only parameter. For MeF and MeBF, the quantum yields are known,[15,17] so that there is no free fit parameter. In these cases, additional fits treating ϕ_{ZE} deliberately as free parameter allow to confirm the validity of the approach. This gave $\phi_{ZE}(\mathrm{MeF}) = 0.11(2)$ and $\phi_{ZE}(\mathrm{MeBF}) = 0.11(2)$ in good agreement with literature.[15,17] Therefore, the fitted values of ϕ_{ZE} for iPrF and 7rF, where no static values are available to compare with, should also be qualitatively correct. Both are in the expected range considering known quantum yields for fulgide derivatives with alkyl substituents at the C^4 position.[8,15,17] A slightly ($\approx 15°$) smaller dihedral angle at the $C^4{=}C^5$ double bond due to the intramolecular bridge[18] might be the reason for the moderately higher quantum yield in case of Z-7rF.

(v) Eventually, the weak oscillations present in the red and blue wing of the ground state absorption band show reversed signs. However, except for Z-MeF (the molecule with the shortest ESA decay time), the significance of this component is low due to weak amplitudes, rapid damping and high parameter correlation.

4. Discussion

4.1. Observed ultrafast dynamics

The spectro-temporal absorption maps and transient decay curves in the previous section provide detailed information on the photo-induced dynamics of the Z-isomers of the fulgide derivatives MeF, iPrF, 7rF, and MeBF. In spite of their different chemical structures, the behaviour of all four Z-fulgides is very similar. In particular, ESA indicates an extremely fast excited-state decay, which is followed by an impulsive rise of HGSA that evidences the wave-packet character of the molecular dynamics. The experimental results agree well with the observed behaviour in our previous study of Z-MeF with excitation at $\lambda_{\mathrm{pump}} = 387$ nm in the red wing of the first absorption band,[25] where however the data were described by a single-exponential ESA decay superimposed with an low-frequency oscillation. At that time, an interpretation as excited-state vibrational coherence involving a low-frequency torsional motion of the furyl unit seemed reasonable, given that a similar oscillatory behaviour had been observed and interpreted in the same way in time-resolved studies of other $E \to Z$ photoisomerisation reactions.[31,32]

The present comparative study of four different Z-furylfulgides with a probe wavelength range extending ≈ 100 nm further into the UV and an improved temporal resolution suggests, however, that the seemingly oscillatory feature rather arises from the delayed impulsive HGSA rise. The present data analysis is in line with the model used for the $Z \to E$ isomerisation of biomimetic dipolar NAIP photoswitches, which isomerise directly via a conical intersection (CI) between the photo-excited state and the electronic ground state and show clear signatures of wave-packet dynamics including a prominent vibrational coherence in the electronic ground state.[28–30]

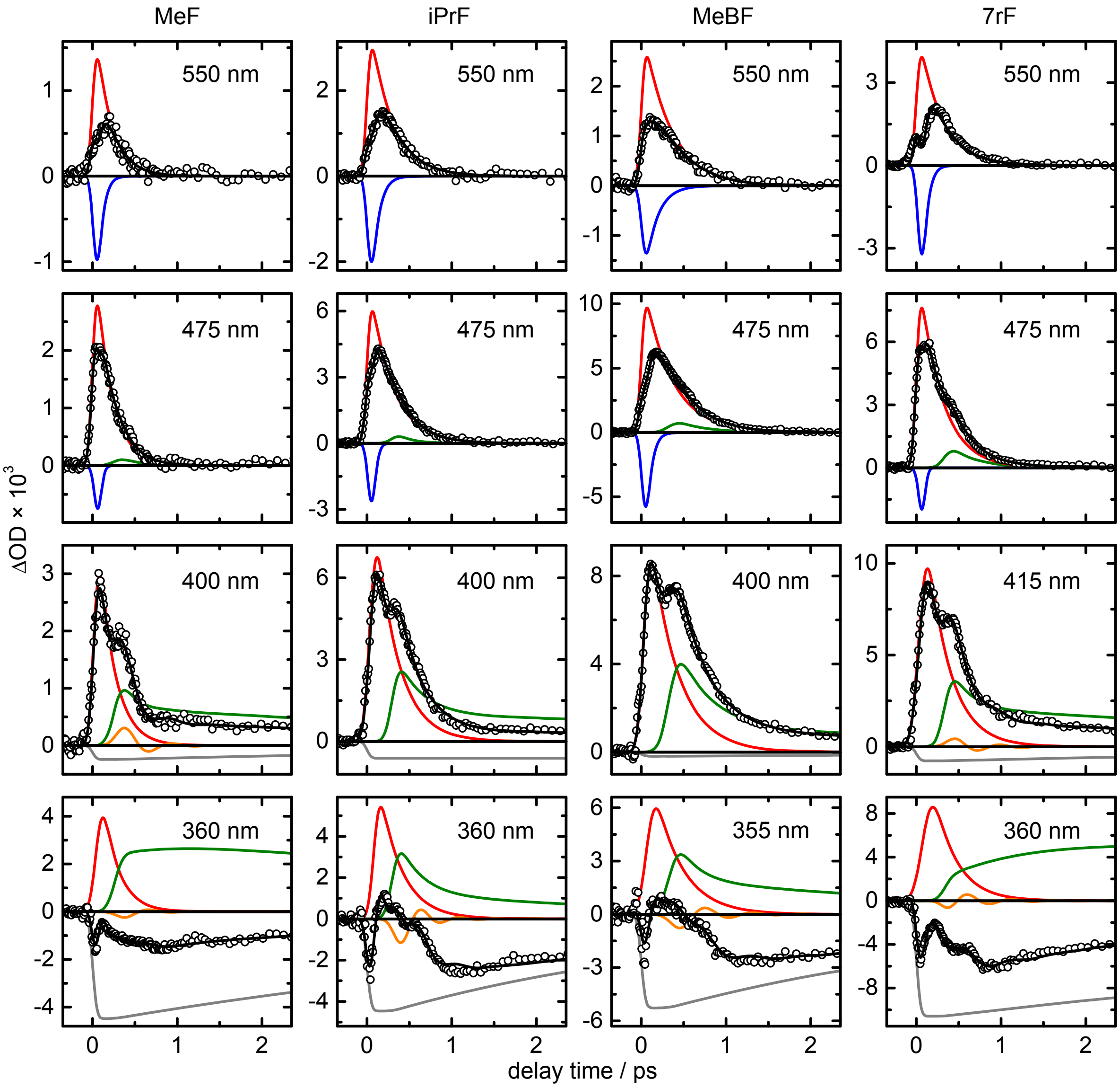

Fig. 5: Transient absorption traces at selected probe wavelengths following excitation of Z-forms of MeF, iPrF, MeBF and 7rF at $\lambda_{\rm pump} = 350$ nm. Open circles represent the data points, black lines the overall fits, coloured lines the contributions of ESA (red), HGSA (green), SE (blue), and ground state absorption (gray). Weak oscillatory components are sketched as orange line.

4.2. Photoisomerisation pathways

The short excited-state lifetimes ($\tau_1 = 0.18 - 0.32$ ps) and the impulsive rise of HGSA provide strong evidence that the $Z \rightarrow E$ photoisomerisation reaction of all four Z-fulgides is a direct process that proceeds on a barrierless excited-state pathway with steep downhill potential energy gradients. The apparent fast spectral blue-shift of the ESA at UV probe wavelengths and the characteristics of the hidden SE band at longer probe wavelengths obtained through the quantitative data analysis corroborate this picture. In line with the general picture of ultrafast photo-induced reactions,[33,34] an efficient photochemical funnel for rapid internal conversion to the electronic ground state is presumably provided by a CI. As in other ultrafast $Z \rightarrow E$ photoisomerisation reactions,[28,29,33–35] the relevant reaction coordinate is most likely a torsional motion corresponding to a change in the dihedral angle formed by the $C^4{=}C^5$ double bond and the adjacent carbon atoms, with the CI located halfway at about 90°. Furthermore, a significant part of the structural rearrangements happen after return to the electronic ground state. Rather than the excited-state lifetime, the time taken for the full development of the HGSA that ranges from ≈ 0.4 ps for MeF to ≈ 0.5 ps for MeBF should thus be interpreted as isomerisation time. This has previously been discussed the same way for the case of the photo-excited NAIP switches, where an isomerisation time of 0.38 ps was found.[28,29]

Figure 6 illustrates the scenario, where the ultrashort

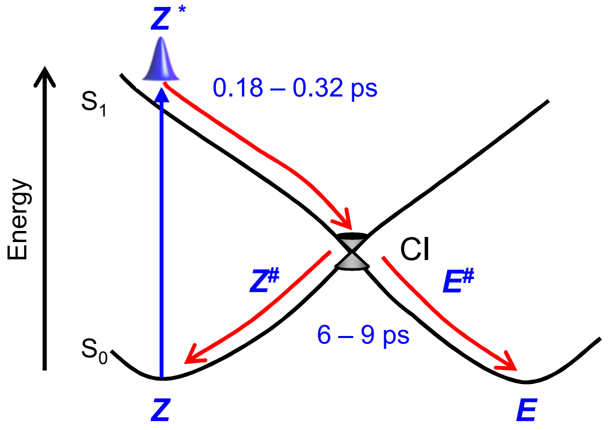

Fig. 6: Sketch of the potential energy hypersurfaces illustrating the $Z \rightarrow E$ photoisomerisation reaction (see text).

pump pulse creates a wavepacket in the FC region of the excited state (Z^* molecules) initially, followed by a fast and directed motion towards the CI, where internal conversion to the electronic ground state takes place. This yields vibrationally hot $E^{\#}$ and $Z^{\#}$ molecules that subsequently undergo vibrational cooling on a much slower time scale. Since the UV/VIS absorption spectra of both isomers are fairly similar, the corresponding HGSA decay cannot be assigned to the individual isomers, however, HGSA of Z-isomers should be dominant considering the low isomerisation quantum yield.

The scenario is further supported by recent state-averaged CASSCF/CASPT2 calculations for photo-excited Z-MeF, where converged S_1-S_0 CI structures could be obtained.[24] The distinctive feature of the CI structures is a twist along the $C^4{=}C^5$ double bond corresponding to a dihedral angle of 90° in line with the scenario suggested above. The proposed direct photoisomerisation of Z-fulgides differs from the accepted model for the $E \rightarrow Z$ photoisomerisation of unpolar polyenes including hexatriene (HT) via an optically dark intermediate state,[36–45] but is in line with the suggested situation for biomimetic dipolar NAIP photoswitches, where the photo-excited state is zwitterionic.[28–30] A similar character of the optically excited state of Z-fulgides seems plausible in analogy to the E-fulgides, for which the applicability of HT as model system has been questioned recently, too.[16,19,21,22,46] The impulsive delayed rise of HGSA indicates that the excited-state wave packet prepared by the ultrashort excitation pulse persists even after passage through the CI. The dynamics directly after return to the electronic ground state is reflected by the fast initial spectral shifts of the HGSA band for probe wavelengths $\lambda_{\text{probe}} \geq 420$ nm. The corresponding values $\tau_2 \approx \tau_1$ are consistent with fast wave packet motion along a steep gradient in the vicinity of the CI. Finally, the signatures of a ground-state vibrational coherence are less pronounced for the Z-fulgides compared to the NAIP photoswitches, but the obvious accordance in the other aspects lends the data analysis some credibility.

4.3. Effects of structural modifications

Previous experimental and theoretical studies of the selected fulgide derivatives were able to relate the observed significant changes in the photoswitching behaviour of the respective E- and C-isomers to details of the ultrafast photo-induced dynamics affected by steric constraints at the central HT unit, intramolecular bridging, or by extension of the π-electron system of the furyl unit.[10,16,19–24] However, the only apparent effect of the structural modifications for the photo-excited Z-fulgides is a moderate slowing of the excited-state dynamics, with time constants ranging from $\tau_1 = 0.18$ ps for Z-MeF to $\tau_1 = 0.32$ ps for Z-MeBF. The very similar results for all four photo-excited Z-isomers indicate that the underlying $Z \rightarrow E$ photoisomerisation mechanism remains unaltered by the structural changes. This is plausible, since torsion about the $C^4{=}C^5$ double bond, the relevant reaction coordinate for the $Z \rightarrow E$ isomerisation,[33] is not sterically hindered considering the equilibrium (X-ray) structures of the Z-isomers.[17,47] Further, the $Z \rightarrow E$ isomerisation is not likely to be affected by the equilibria between the Z_α and Z_β conformers of the studied derivatives either.[16] Even benzannulation does not seem to induce significant changes of the excited-state potential energy hypersurfaces governing the $Z \rightarrow E$ photoisomerisation. Rather, the observed moderate increase of the isomerisation times for the larger Z-fulgides, in particular Z-MeBF, is likely to be caused by the larger size of the momenta and increased solvent friction considering that torsion about the $C^4{=}C^5$ double bond requires a large-amplitude motion.

5. Conclusions

In conclusion, we have performed a comparative femtosecond time-resolved transient absorption study of the photo-induced dynamics of four structurally modified Z-fulgides in n-hexane after excitation at $\lambda_{\text{pump}} = 350$ nm. The detailed picture provided by the present results indicates that the photoisomerisation of Z-fulgides is a fast and direct process along barrierless excited-state pathways with lifetimes ranging from $\tau_1 = 0.18$ ps for Z-MeF to $\tau_1 = 0.32$ ps in the case of Z-MeBF. The deactivation/isomerisation to the electronic ground states of the Z- and E-isomers proceeds via a CI and results in an impulsive appearance of HGSA. This shows that the wave packet initially prepared by the ultrashort laser pulse in the Franck-Condon region of the photo-excited state survives passage into the electronic ground state. Furthermore, the results provide qualitative evidence for a quickly dephasing vibrational coherence in the electronic ground state. In contrast to the significant changes observed for the corresponding E- and C-isomers,[17,19,20] the excited-state dynamics of the Z-isomers is affected only little by steric hindrance at the central HT unit, intramolecular bridging, or by extending the π-electron system via benzannulation of the furyl ring. The photoisomerisation of Z-fulgides thus appears as an extremely fast and robust photoreaction that prevents accumulation of the unwanted Z-isomers and ensures optical bistability of fulgide photoswitches irrespective of structural modifications, with significant importance regarding chemical tuning for improved applications.

Acknowledgments

This work has been supported by the Deutsche Forschungsgemeinschaft (DFG) through sub-project A1 of the SFB 677 "Function by Switching" (RS, FR, FT) as well as by the Biophotonics Initiative (Grant no. 13N9234) of the German Ministry of Research and Education (FS, JM) and by a research grant of the DFG (FS, JM).

[1] *Molecular Switches*, ed. B. L. Feringa, Wiley-VCH, Weinheim, 2001.
[2] H. Rau, in *Photochromism: Molecules and Systems*, ed. H. Dürr and H. Bouas-Laurent, Elsevier, Amsterdam, 2003.
[3] S. Kawata and Y. Kawata, *Chem. Rev.*, 2000, **100**, 1777–1788.
[4] J. Andréasson and U. Pischel, *Chem. Soc. Rev.*, 2010, **39**, 174–188.
[5] S. W. Hell, *Science*, 2007, **316**, 1153–1158.
[6] D. Gust, J. Andréasson, U. Pischel, T. A. Moore and A. L. Moore, *Chem. Commun.*, 2012, **48**, 1947–1957.
[7] H. G. Heller and S. Oliver, *J. Chem. Soc., Perkin Trans. 1*, 1981, 197–201.
[8] Y. Yokoyama, *Chem. Rev.*, 2000, **100**, 1717–1739.
[9] Y. Yokoyama, *New J. Chem.*, 2009, **33**, 1314–1319.
[10] F. Renth, R. Siewertsen and F. Temps, *Int. Rev. Phys. Chem.*, 2013, **32**, 1–38.
[11] Y. Yokoyama, T. Goto, T. Inoue, M. Yokoyama and Y. Kurita, *Chem. Lett.*, 1988, **17**, 1049–1052.
[12] Y. Yokoyama, T. Inoue, M. Yokoyama, T. Goto, T. Iwai, N. Kera, I. Hitomi and Y. Kurita, *Bull. Chem. Soc. Jpn.*, 1994, **67**, 3297–3303.
[13] Y. Liang, A. S. Dvornikov and P. M. Rentzepis, *J. Mater. Chem.*, 2000, **10**, 2477–2482.
[14] M. A. Wolak, C. J. Thomas, N. B. Gillespie, R. R. Birge and W. J. Lees, *J. Org. Chem.*, 2003, **68**, 319–326.
[15] E. Uhlmann and G. Gauglitz, *J. Photochem. Photobiol. A*, 1996, **98**, 45–49.
[16] R. Siewertsen, F. Renth, F. Temps and F. Sönnichsen, *Phys. Chem. Chem. Phys.*, 2009, **11**, 5952–5961.
[17] F. Strübe, R. Siewertsen, F. D. Sönnichsen, F. Renth, F. Temps and J. Mattay, *Eur. J. Org. Chem.*, 2011, 1947–1955.
[18] F. Strübe, J. Mattay, B. Neumann and H. G. Stammler, *Acta. Crystallogr. C*, 2011, **67**, o33 – o36.
[19] R. Siewertsen, F. Strübe, J. Mattay, F. Renth and F. Temps, *Phys. Chem. Chem. Phys.*, 2011, **13**, 3800–3808.
[20] R. Siewertsen, F. Strübe, J. Mattay, F. Renth and F. Temps, *Phys. Chem. Chem. Phys.*, 2011, **13**, 15699–15707.
[21] J. B. Schönborn, J. Sielk and B. Hartke, *J. Phys. Chem. A*, 2010, **114**, 4036–4044.
[22] J. B. Schönborn, A. Koslowski, W. Thiel and B. Hartke, *Phys. Chem. Chem. Phys.*, 2012, **14**, 12193–12201.
[23] J. B. Schönborn and B. Hartke, *J. Photochem. Photobiol. A*, 2013, **263**, 34–40.
[24] J. B. Schönborn and B. Hartke, *Phys. Chem. Chem. Phys.*, 2014, **16**, 2483–2490.
[25] F. Renth, M. Foca, A. Petter and F. Temps, *Chem. Phys. Lett.*, 2006, **428**, 62–67.
[26] To display the transient absorption maps with optimal dynamic ranges, they are plotted using a logarithmic scale by taking $\log(1 + \Delta t/\mathrm{ps})$. The plot scale was then relabeled to correctly range from $\Delta t = -0.25$ to 30 ps.
[27] I. H. M. van Stokkum, D. H. Larsen and R. van Grondelle, *Biochim. Biophys. Acta*, 2004, **1657**, 82104.
[28] J. Briand, O. Bräm, J. Réhault, J. Léonard, A. Cannizzo, M. Chergui, V. Zanirato, M. Olivucci, J. Helbing and S. Haacke, *Phys. Chem. Chem. Phys.*, 2010, **12**, 3178–3187.
[29] J. Léonard, I. Schapiro, J. Briand, S. Fusi, R. R. Paccani, M. Olivucci and S. Haacke, *Chem. Eur. J.*, 2012, **18**, 15296–15304.
[30] J. Léonard, J. Briand, S. Fusi, V. Zanirato, M. Olivucci and S. Haacke, *N. J. Phys.*, 2013, **15**, 105022.
[31] S. Takeuchi and T. Tahara, *Chem. Phys. Lett.*, 2000, **326**, 430–438.
[32] B. Hou, N. Friedman, M. Ottolenghi, M. Sheves and S. Ruhman, *Chem. Phys. Lett.*, 2003, **381**, 549–555.
[33] B. G. Levine and T. J. Martinez, *Annu. Rev. Phys. Chem.*, 2007, **58**, 613–634.
[34] *Conical Intersections II: Theory, Computation and Experiment*, ed. W. Domcke, D. R. Yarkony and H. Köppel, World Scientific, Singapore, 2011.
[35] R. Siewertsen, J. B. Schönborn, B. Hartke, F. Renth and F. Temps, *Phys. Chem. Chem. Phys.*, 2011, **13**, 1054–1063.
[36] D. R. Cyr and C. C. Hayden, *J. Chem. Phys.*, 1996, **104**, 771–774.
[37] P. Celani, F. Bernardi, M. A. Robb and M. Olivucci, *J. Phys. Chem.*, 1996, **100**, 19364–19366.
[38] S. Lochbrunner, W. Fuß, K.-L. Kompa and W. E. Schmid, *Chem. Phys. Lett.*, 1997, **274**, 491–498.
[39] K. Ohta, Y. Naitoh, K. Tominaga, N. Hirota and Y. Keitaro, *J. Phys. Chem. A*, 1998, **102**, 35–44.
[40] S. Lochbrunner, W. Fuß, W. E. Schmid and K.-L. Kompa, *J. Phys. Chem. A*, 1998, **102**, 9334–9344.
[41] M. Boggio-Pasqua, M. J. Bearpark, M. Klene and M. A. Robb, *J. Chem. Phys.*, 2004, **120**, 7849–7860.
[42] J. Catalán and J. L. G. de Paz, *J. Chem. Phys.*, 2006, **124**,

034306.
[43] A. Nenov, T. Cordes, T. T. Herzog, W. Zinth and R. de Vivie-Riedle, *J. Phys. Chem. A*, 2010, **114**, 13016–13030.
[44] F. Bernardi, M. Olivucci and M. A. Robb, *Chem. Soc. Rev.*, 1996, **25**, 321–328.
[45] W. Fuß, Y. Haas and S. Zilberg, *Chem. Phys.*, 2000, **259**, 273–295.
[46] G. Tomasello, M. J. Bearpark, M. A. Robb, G. Orlandi and M. Garavelli, *Angew. Chem. Int. Ed.*, 2010, **122**, 2975–2978.
[47] Y. Yoshioka, T. Tanaka, M. Sawada and M. Irie, *Chem. Lett.*, 1989, **19**, 19 – 22.